Journal of King Saud University – Science 35 (2023) 102708

HOSTED BY

Contents lists available at ScienceDirect

Journal of King Saud University – Science

journal homepage: www.sciencedirect.com

Original article

Anticancer potentiality of green synthesized Mg-Co ferrites nanoparticles against human breast cancer MCF-7 cells

Naushad Ahmad [a,*], Suliman Yousef Alomar [b,*], Fadwa Albalawi [b], Mohammad Rizwan Khan [a], Nida Nayyar Farshori [c], Rizwan Wahab [b], Mohammed Rafi Shaik [a]

[a] Department of Chemistry, College of Science, King Saud University, Riyadh 11451, Saudi Arabia
[b] Department of Zoology, College of Science, King Saud University, Riyadh 11451, Saudi Arabia
[c] Department of Pharmacognosy, College of Pharmacy, King Saud University, Riyadh 11495, Saudi Arabia

ARTICLE INFO

Article history:
Received 17 February 2023
Revised 20 April 2023
Accepted 30 April 2023
Available online 8 May 2023

Keywords:
Ferrites
Crystal structure
Morphology
Optical
Cytotoxicity
ROS
MCF-7

ABSTRACT

Inherent magnetic features of engineered nanomaterials are quite important parameters for biomedical applications and cancer treatments. In this study, cobalt ferrite (CF-NPs) and magnesium-cobalt ferrite (MCF-NPs) magnetic nanoparticles were synthesized by aqueous extract of turmeric, characterized by various instruments, and utilized for anticancer activity. These are characterized with TG-DTG, XRD, SEM, BET, FTIR, and UV–Vis sophisticated techniques. The results revealed that they have inverse cubic spinel structure, optically active and nanoscale spherical morphology. The particle size was calculated by the Scherrer formula and was found to be 24.78 nm for CF-NPs and 27.48 nm for MCF-NPs, respectively. Moreover, MTT method was used to find out anticancer activity of the fabricated CF-NPs and MCF-NPs using the human breast cancer cells (MCF-7) and data discloses that cytotoxicity effects of CF-NPs are higher than MCF-NPs, and dose dependent. At high dose (100 μg/ml), CF-NPs shows 45.76% and 61.57% in CF-NPs and MCF-NPs cell viability, respectively. Similarly, cellular ROS generation was found to be higher in CF-NPs (183 %) as compared to MCF-NPs (159% in at 100 μg/ml). By the obtained results it can be claimed that ferrites will be useful model for cancer treatments if they are explored at advance level.

1. Introduction

In the current scenario, magnetic nanoparticles (MNPs) connected with various medical applications have been found a special attention on account of their ecofriendly abundance in nature, high surface-to-volume ratio, fast reactivity with biomolecules, and greater opportunity to surface functionalization (Issa et al., 2013). Due to the peculiar magnetic properties, these have incredible binding interaction with DNA, enzymes, peptides, antibodies, and high dispersion in blood and cellular fluid which help in diagnosis of diseases and delivery of drugs at targeted sites in the presence of magnetic field (Issa et al., 2013; Andrade et al., 2020). Therefore, these are considering as suitable and biocompatible candidates for the treatments of hyperthermia/ thermotherapies, iron deficiency, and cancer; and technologically useful for the fabrication of many sophisticated devices like sensors, detectors, magnetic energy storages, and MRI (Issa et al., 2013; Andrade et al., 2020; Wu and Huang, 2017).

Magnetic Spinel ferrite NPs (Fe_3O_4) have been extensively studied for many clinical analyses however, due to limitation of their attributes such as low magnetization, particle agglomeration and rapid reactions (Mathew and Juang, 2007), researcher's attention shifted towards structural ferrites (AB_2O_4, A = M^{2+} and B = M^{3+} ions). Structural ferrites are classified into normal, inverse, and mixed spinel metal oxides (Jia et al., 2012). A number of cations with various oxidation number/or valence state can be accommodated into the A and B sites by control substitution with other precursors like Metals, Carbons, and MO that tuned features into reasonable domain and provide platform for the fabrication of a finely dispersed and biocompatible nano-size materials (Jia et al., 2012; Zutic et al., 2004). AFe_2O_4 based spinel ferrites with "A"

* Corresponding authors.
E-mail addresses: anaushad@ksu.edu.sa (N. Ahmad), syalomar@ksu.edu.sa (S.Y. Alomar).

Peer review under responsibility of King Saud University.

Production and hosting by Elsevier

https://doi.org/10.1016/j.jksus.2023.102708
1018-3647/

variation (like Mg, Zn, Cu, Mn, Ni, and Co) possess good magnetic, optical, and electrical properties that remain important in field of biomedical applications and modern technologies (Jia et al., 2012; Zutic et al., 2004; Carta et al., 2009).

In recent years, AFe_2O_4 type of nano-ferrites have generated high curiosity in the delivery of drugs and treatment of various cancerous cells due to significantly improved magnetic and surface properties (Pon-On et al., 2011). Till date, more than 100 different types of cancer are observed, therein, breast cancer is very common particularly in females (Chen et al., 2020; Wahab et al. 2014). If it is passes with initiation, promotion, and progression phases, then it is difficult to control on growth. However, magnetic and structural ferrites NPs are the right preventive option to control their growth and multiplication of cancer cell because of more production of free radicals, bestowed favors to kill the cancer cell selectively than others, and have a greater ability to deliver the anticancer drugs with minimal side-effect on healthy tissues and organs, main challenge of cancer treatment (Wu and Huang, 2017), Pon-On et al., 2011 and Chen et al., 2020), rather than use of traditional and non-selective therapies for instance chemotherapy, radiotherapy, proton beam therapy, drug therapy, immune therapy, surgery, and clinical trials etc., that impact high pains and suffering (Bray et al., 2012; Nardin et al.2020). The cells viability is much influences by ROS generation, which is the most probable mechanism through which NPs induce cytotoxicity. It is reported in literature, that small metallic NPs lesser than 50 nm size revealed an outstanding curative attributes and features against the corresponding cancer cell lines because of superior entering into cells and significantly higher anti-cancer activities as compared to bigger size NPs (You et al.2012).

Cobalt ferrite ($CoFe_2O_4$) NPs provides a number of utilities in several fields such as food, medicine, cancer treatment and others. Its relies on the striking features of ferrite such as shape, size, concentrations of the NPs. To date, $CoFe_2O_4$NPs are usually synthesized by co-precipitation, hydrothermal, microwave, solid-state, combustion and emulsion approaches (Jia et al., 2012; Carta et al., 2009). Nevertheless, these processes are often completed at raised temperatures and pressures, complicated tools and procedures, and toxic solvents and chemical that result in enhanced energy demand and environmental costs (Ashour et al., 2018). Hence, there is a highest obligation to get the better of these disadvantages by finding an alternative green approaches (Moradiya et al., 2021; Kombaiah et al., 2018; Taj et al., 2021). A few reports are accessible for the biological application of $CoFe_2O_4$ NPs and its derivatives to reduce the rate of cancer cells growth. Therefore, in the present study our aimed to fabricate $Co_{1-x}Mg_xFe_2O_4$ ferrite nanoparticles by aqueous extract of turmeric powder, to investigate their structural, morphological and cytotoxic evaluation of MCF-7 cell line.

2. Materials and methods

2.1. Biogenic synthesis of ferrite nanoparticles

Cobalt ferrite ($CoFe_2O_4$, CF-NPs) and Mg-doped cobalt ferrite nanoparticles ($Co_{0.95}$ $Mg_{0.05}$ Fe_2O_4, MCF-NPs) were formed via green process with utilization of aqueous extract of turmeric powder. About 5gm sun-dried turmeric yellow powder was placed in 100 mL deionized water, boiled for 15 min, then filtered to room temperature at room temperature. The pH of extract was measured and found to be 6.24, and finally used for fabrication of ferrites.

CF-NPs was fabricated by mixing cobalt (II) nitrate ($Co(NO_3)_2$·$6H_2O$, Sigma-Aldrich, USA) with iron (III) nitrate ($Fe(NO_3)_3$·$9H_2O$, Sigma-Aldrich, USA) in the molar ratio of 1:2 as precursor. Both precursors were completely liquefied and dissolved in distilled water and then added dropwise into 50 mL aqueous extract under fast stirring for 60 min. Further it was heated at 90 °C until turned to dark color for complete reduction process. Then it was cooled overnight where a dark precipitate started to appear, signifies the beginning of nanoparticles formation. The precipitate was dried for 12 h at 110 °C. The dried sample was heated in the furnace at the rate of 10 °C/min in air atmosphere for 6 h at 750 °C. The color of calcined sample was dark black. MCF-NPs of light black color was obtained by the same procedure as for the CF-NPs using metal nitrates in a ratio of 0.05 Mg^{2+}:0.95Co^{2+}:2Fe^{3+} and 50 mL extract.

2.2. Characterizations of Mg-Co ferrites nanoparticles

Thermogravimetric analyses of ferrospinel precursors were performed on Q600 SDT-TA Instruments (Champaign, USA) in the temperature range of 25–900 °C in oxidative condition at the flow rate of 20 mL min^{-1}. To analyze the crystal phase and purity of ferrites NPs, X-ray diffraction (XRD, Westborough, MA, USA) equipped by Ni filter using radiations source of $Cu_{K\alpha}$ (λ = 1.54056 Å). Using the KBr method, functional groups were determined with the help of IRAffinity-1 FTIR spectrophotometer (Shimadzu, Japan) and spectra were recorded at 400–4000 cm^{-1}. UV–Visible spectra of aqueous solution were carried out by UV–Visible spectrophotometer (Thermo Fisher Scientific, USA). The surface properties were determined by BET method on Micromeretics Tristar 2000 instrument (Norcross, USA). The morphology was observed via scanning electron microscopy (SEM, JEM-2100F; JEOL, Japan).

2.3. Anticancer activity

2.3.1. Reagents and consumables for anticancer activity

2,7-dichloro dihydrofluorescein diacetate (DCFH-DA) and 3-(4, 5-dimethylthiazol-2-yl)-2,5-diphenyltetrazolium bromide (MTT) were obtained from Sigma-Aldrich, USA. Dulbecco's Modified Eagle Medium (DMEM) as a culture medium, antibiotics-antimycotic, 10% FBS, and sodium bicarbonate ($NaHCO_3$) were purchased from Invitrogen, USA. The flat well plates, micropipets, bottles and other consumables items were used from Nunc (A/S), Denmark.

2.3.2. Cell culture

The MCF-7 cells were cultured in DMEM using 10% FBS, 0.2% $NaHCO_3$, and antibiotic/antimycotic solution (100×,1 mL/100 mL of medium). The cells were preserved in 5% CO_2 and 95% O_2 in humid atmosphere and 37 °C and greater than 98% cells viability was achieved through trypan blue test.

2.3.3. Cytotoxicity measurement

The cells (MCF-7) were exposed with a varied concentrations of NPs (1–100 μg/ml in PBS) for 24 h, and cytotoxicity of treated cells (1×10^4) was measured by MTT assay. Briefly, these cells were allowed to follow for 24 h in 5% CO_2 incubator at 37 °C in 96 well culture plates. Once the treatment was completed, MTT (5 ppm of stock in PBS) was added (10 μl/well in 100 μl of cell suspension) in each well and plates were further incubated for 4 h in incubator at 37 °C. Thereafter, supernatant was cast out, and DMSO (50 μl) were gently added to each well. The developed color was read at 550 nm with ELISA microplate reader (BioTek, USA). Similarly, untreated sets as control were read under the same conditions. The percentage (%) viability of cells was calculated by equation:

$$\text{Viability } (\%) = [(\text{total cells} - \text{viable cells})/\text{total cells})] \times 100$$

2.3.4. Morphological analysis

The changes in cells (MCF-7) structures were observed to analyzed the alterations in the presence of NPs. The cells were treated with different concentrations (25, 50 and 100 μg/mL in PBS) of NPs

for 24 h and the morphological changes in the cells at 20 × magnification were carried out using inverted phase contrast microscope.

2.3.5. ROS measurement

Cellular ROS of fabricated ferrites was measured using fluorescence dye, DCFH-DA. After the treatment of ferrites (25, 50 and 100 μg/mL in PBS) with the MCF-7 cells for 24 h, they had been treated with DCFH-DA (20 μM) at 37 °C and 5% CO_2 for 1 h in dark. Then ROS of treated and untreated cells were visualized under fluorescence microscope.

2.3.6. Statistical analysis

The statistical determination was depicted with the standard $p < 0.05$ value, which were considered as statistically significant.

3. Results

3.1. Thermal study of precursors

To know the final calcination temperature for the formation of crystalline phase, thermal analyses were performed on the ferrospinel precursors under air atmosphere. DTG peaks (Fig. 1) are helped to get evidence for the removal of associated solvent, molecules and amorphous to crystalline phase transformation by temperature maxima (T_{max}). Both precursors showed two steps decompositions. The CF-precursor showed the first T_{max} peak at around 125 °C due to the evaporation of adsorbed humidity and hydrates on the surface (Amiri and Shokrollahi, 2013). The second T_{max} peak at 307 °C, (the first T_{max} peak in MCF- precursor) can be associated with the decomposition of the nitrates, available organic moieties of turmeric, and initiation of crystallization process (Prasanna et al., 2015). The second T_{max} peak at 610 °C in MCF-precursor showed completely removal of attached organic groups. Therefore, the calcination temperature of the precursors was specified by 700 °C for the formation of expected metal ferrites, because there are no any major changes observed after heating at high temperature ($T \leq 800$ °C).

3.2. XRD study

To examine the calcined ferrites NPs structure, the XRD measurements were implemented, shown in Fig. 2. The diffraction peaks at 30.11°, 35.45°, 37.05°, 43.03°, 53.51°, and 56.97° can be indexed as the (220), (311), (222), (400), (422), and (511) planes in the XRD pattern confirms the inverse cubic spinel type structure of the formed NPs with space group fd_3m. The entire diffraction

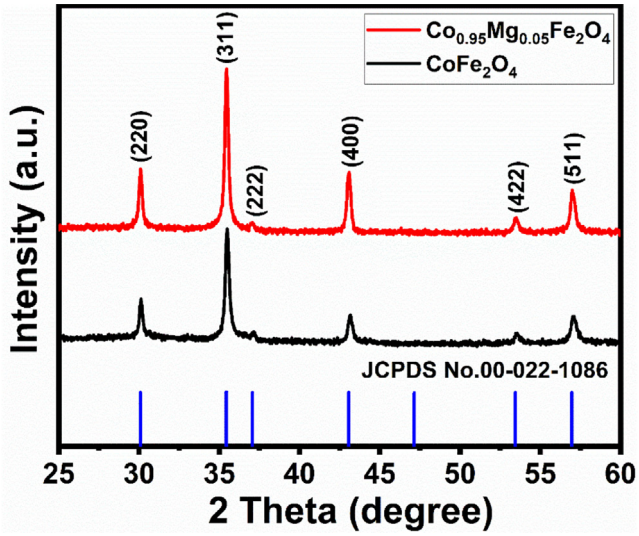

Fig. 2. X-ray diffraction patterns of the ferrite nanoparticles.

pattern was well matched with the $CoFe_2O_4$ phase and analogous with the available standard JCPDS card No. 00-022-1086 (Monogr 1971) with lattice parameter is 8.3919 Å. The crystallite size of the synthesized NPs was calculated using the Scherrer equation (Kumar et al 2013). It is defined as:

$$D = k\lambda/\beta\cos\theta$$

where constant k depends upon the shape of the crystallite size (k = 0.89, assuming the circular grain), λ is the wavelength of the CuK_α radiation (λ = 0.1542 nm), β is the Full Width Half Maximum (FWHM) in radians, θ is Braggs's diffraction angle and D is the crystallite size. Using the FWHM of the most intense peak corresponding to the (311) plane, the crystallite size was obtained 24.78 nm for CF-NPs and 27.48 nm for MCF-NPs, respectively.

3.3. FT-IR study

The FT-IR spectra of the NPs, to analyze their purity, are shown in Fig. 3. The CF-NPs showed an absorption peak at 464.95 cm^{-1}, which is not appeared in MCF-NPs, and other peak between 593 and 567 cm^{-1} are attributed to intrinsic lattice vibrations of octahedral (long band length of oxygen-metals) and tetrahedral sites (shorter band length of oxygen-metals) in the spinel structure (West, 1984; Villete et al., 1998). The peaks between 1400 and 1300 cm^{-1} and 900–1100 cm^{-1} represented the nitrate ions. An

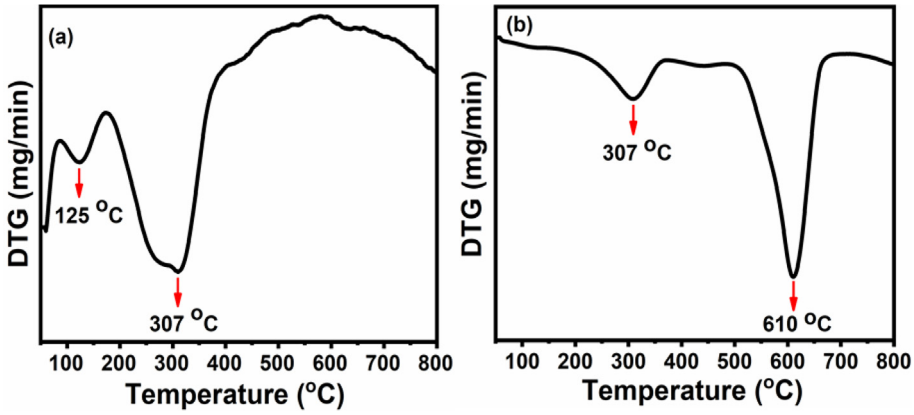

Fig. 1. DTG curves of (a) CF and (b) MCF ferrite precursors.

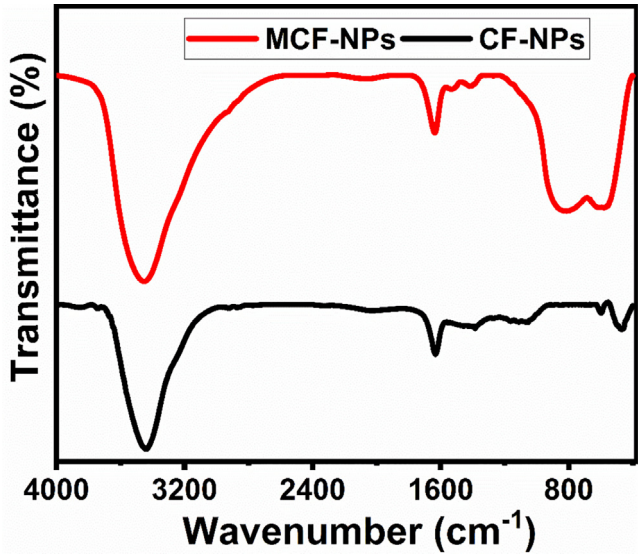

Fig. 3. FT-IR spectra of the ferrite nanoparticles.

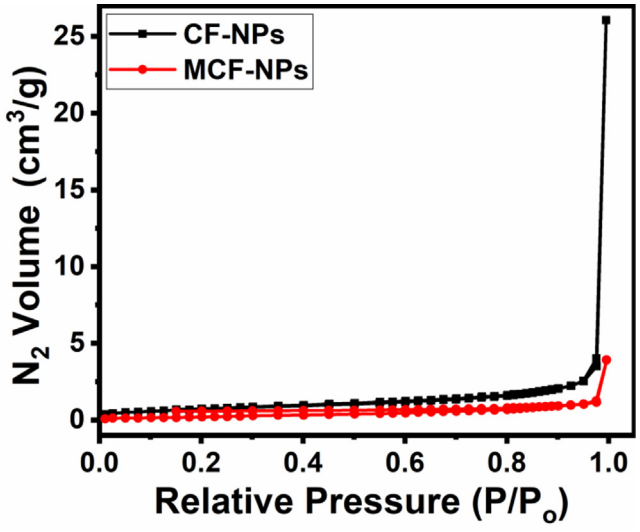

Fig. 5. N_2 adsorption–desorption isotherms of the ferrite nanoparticles.

intense peak at 3447 cm^{-1} and small peak at 1632 cm^{-1} due to the stretching vibrations of water (H–O–H) and hydroxyl ions (O–H) on the surface of NPs, suggesting the polar nature of the surface (Jha and Prasad, 2012).

3.4. UV–Vis study

For the ferrites like other semiconductors, the band gap energy, which is calculated using the formula $E_g = 1240/\lambda_{max}$, where λ_{max} is the absorption in nm, is one of the distinguished factors in most applications as in photovoltaic devices or photo catalysis (Das et al., 2010). UV–vis spectra of CF-NPs and MCF-NPs were displayed in Fig. 4. The spectra of fabricated NPs were observed in visible region which was shifted towards lower wavelength in case of MCF-NPs, from 535 nm to 404 nm, and calculated band gap energy increased. The estimated band gap energy is found 2.31 eV for CF-NPs and 3.06 eV MCF-NPs, respectively.

3.5. BET surface area

The nitrogen adsorption–desorption isotherms of pure and doped ferrites are shown in Fig. 5. Base on the IUPAC designation, they are reflecting mesoporous type IV isotherms and pore diameters are in the range 2–50 nm. The porosity parameters such as BET surface area, pore volume, and average diameter of each pore for prepared degassed samples are tabulated in Table 1. From the table it is clear that Mg^{2+} ion doping in pure $CoFe_2O_4$ ferrite decrease the porosity measurements which was good agreement with XRD and SEM the results.

3.6. Morphological study (SEM)

SEM images were captured to observe the morphology of the fabricated NPs. Fig. 6 (a-b) and (c-d) represented SEM images of the CF-NPs and MCF-NPs at low (x 5000) and high magnifications (x 30000). The low-magnification images (a & c) shows the flakes of nanoparticles in micro-mm range. A closer view of flakes at high magnification (b & d) disclosed that flakes are nearly made of nano-sized with sphere-shaped. The average dimension of CF-NPs is around 20–50 nm which are smaller than MCF-NPs; and these findings are well agreed with the results obtained from XRD data where sharp patterns are the indication of well define crystallization. Therefore, the selected calcination temperature plays major role for the nucleation and growth of CF-NPs that directly reflects the high anticancer activity of CF-NPs. However, MCF-NPs showed irregular morphology besides spherical and agglomeration of strongly connected larger grains because of greater magnetic interactions among the particles. Moreover, it

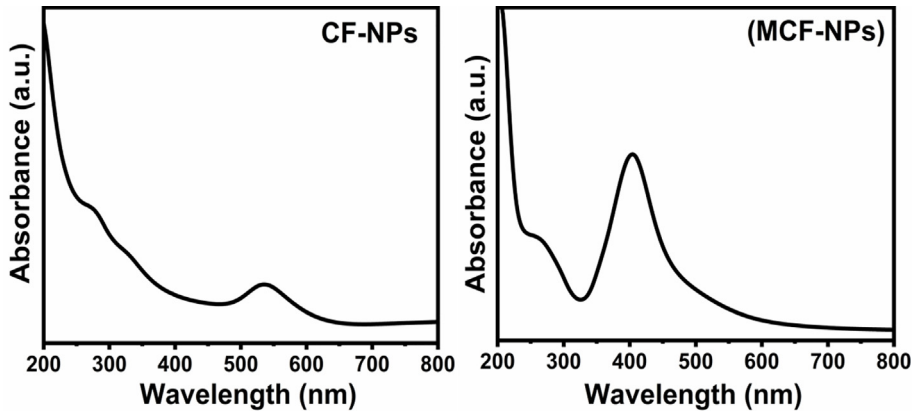

Fig. 4. UV–Vis spectra of the ferrite nanoparticles.

Table 1
Porosity parameters of the synthesized nanoparticles.

Ferrites	Pore Volume (cm^3/g)	Pore size (nm)	Surface area (m^2/g)
CF-NPs	0.040	59.383	2.716
MCF-NPs	0.006	29.793	0.812

should be noted that there are plenty of voids between the nanoparticles.

3.7. Cytotoxicity study

3.7.1. Effect of ferrites NPs on cell viability

As described in section 2.3.3 that the untreated and treated MCF-7 cells with ferrites NPs were treated in a range of 1–100 μg/ml for 24 h incubation. The obtained result via MTT assays are summarized in Fig. 7. It is observed when concentration of fabricated NPs was lower than 25 μg/ml, it was not much affected. However, when the concentrations have increased the cytotoxicity was influenced that is dose dependent. It is found that CF-NPs was more effective than MCF-NPs against the cells. The cell viability was noted to 100.89 %, 60.22% and 45.76% in CF-NPs at 1 μg/ml, 50 μg/ml and 100 μg/ml concentration, respectively. Similarly, in case of MCF-NPs, it was observed to 100.82%, 73.69% and 61.57% at 1 μg/ml, 50 μg/ml and 100 μg/ml concentration, respectively.

3.7.2. Effect of ferrites NPs on cell morphology

The structural changes in MCF-7 cells exposed to NPs at three concentrations, 25, 50 and 100 μg/ml for 24 h incubation periods are shown in Figs. 8 & 9, respectively. The cells indicate that morphological changes after the exposure of NPs are to be concentration dependent, and realized that as the concentrations of NPs upsurges the viability of cells were effectively damaged. In case of CF-NPs, changes in the morphology of MCF-7 cells at low concentration 25 μg/ml does not show remarkable changes in cells morphology, whereas at 50 and 100 μg/ml concentrations of CF-NPs reduced the normal morphology of the cells, the cell adhesion capacity, and the cell density as compared to control. Most of the cells damaged and lost their typical morphology at 100 μg/ml of CF-NPs for 24 h.

3.7.3. Influence of ferrites NPs on ROS generation

To explore the ability of cytotoxicity of both ferrites at various concentrations, we have performed the generation of ROS using DCFH-DA dye. The acquired information is shown in Fig. 10 (a & b). At low concentrations (1 to 10 μg/ml) there are no significant generation of reactive free radicals but at higher concentrations (25 to 100 μg/ml) they are increased accordingly. ROS production was increased 158% to 183% in CF-NPs, whereas 126% to149% in MCF-NPs at 50 and 100 μg/ml, respectively.

4. Discussion

Ferrites MNPs mostly used for the fabrication of valuable devices such as powerful magnets, data storage, biosensors, biomarkers, disks of computers etc. A number of applications of MNPs are described in detail but limited data are available in oncology, a discipline of cancer treatment. In this study, we have prepared CF-NPs and MCF-NPs by biogenic method which shows critical influence on thermal, crystallinity, optical, surface, morphological, and anticancer properties because of present of phytochemicals such as terpenoids and phenolic compounds. To develop the crystal structure, thermal stability and purity of ferrites NPs, calcination temperature and time duration are the important and decision making factors. For this, TG-DTG analyses were applied to investigate decomposition patters on precursors which is quite

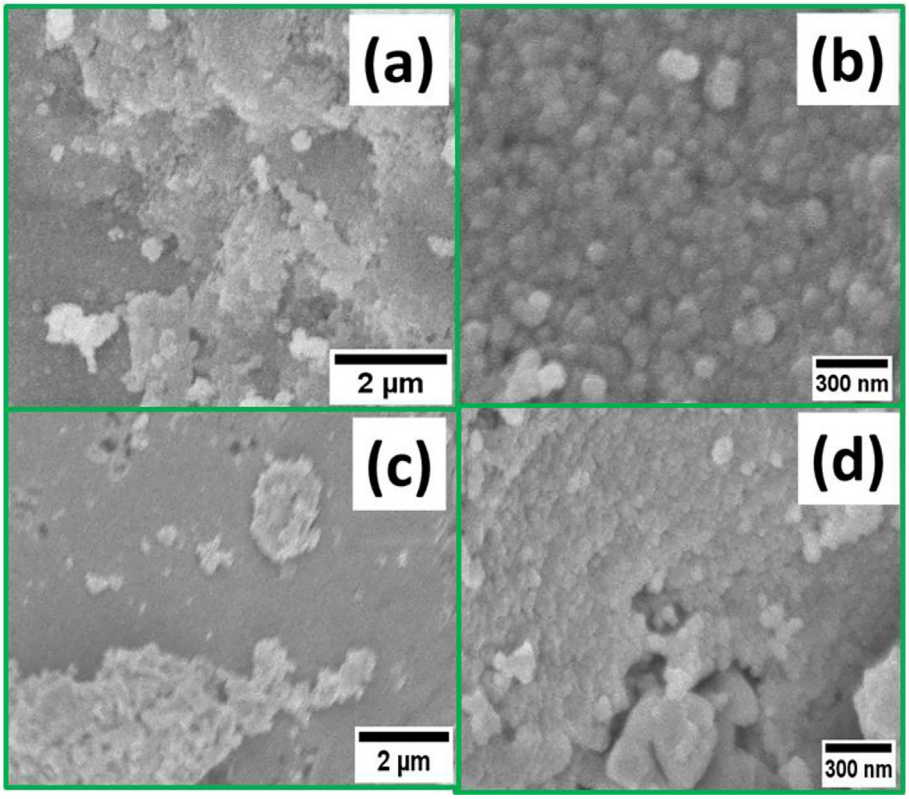

Fig. 6. SEM images of (a-b) CF-NPs and (c-d) MCF-NPs.

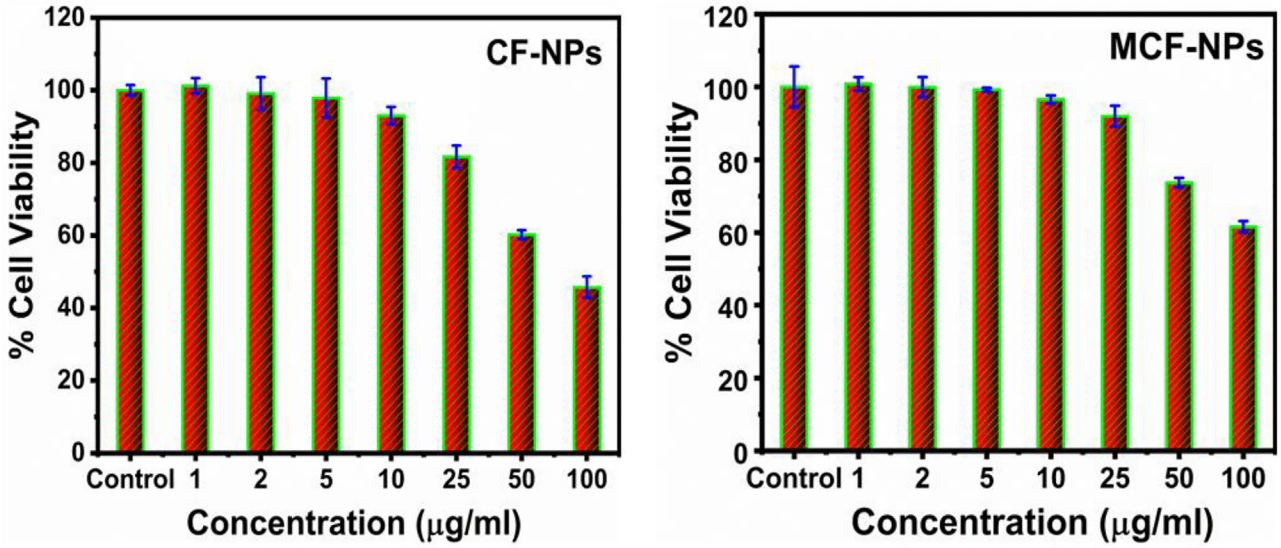

Fig. 7. Cytotoxicity of the ferrites NPs against in MCF-7. The experiments were conducted in triplicate manner (Mean ± SD triplicate).

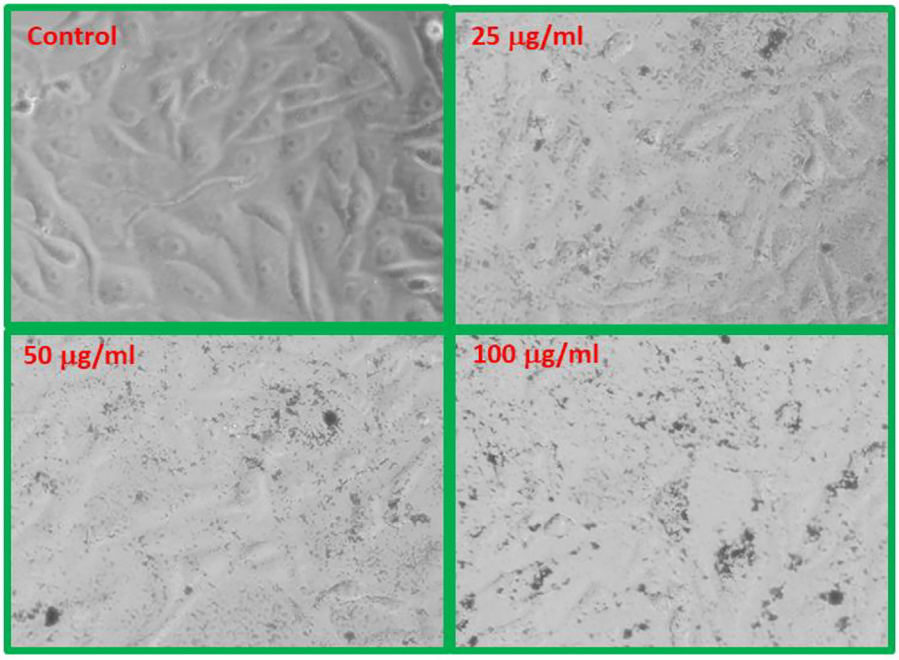

Fig. 8. CF-NPs induced morphological changes in MCF-7 cells.

useful technique to find out the above observations. The degree of crystallinity and crystal size was confirmed by XRD analysis which revealed that the fabricated ferrites are pure and nano-phase materials, 24.78 to 27.48 nm, with inverse cubic spinel type. Thus, selected calcination temperature plays a key role for the cation distributions on both tetrahedral and octahedral sites, nucleation and growth of crystals with striking features. FT-IR spectra are provided information about functional details and redistribution of cations between octahedral and tetrahedral sites into the inverse spinel structures. The optical absorption properties were examined via UV–Vis spectroscopy. The fabricated ferrites show spectra in visible regions and calculated band gap energy was found 2.31 eV for CF-NPs and 3.06 eV MCF-NPs. This variation may arise due the presence of Mg^{2+} ion which changed the electronic state in the outer orbital area, structure, and particle sizes which in turn increased band gap energy (Tehrani et al., 2012; Casbeer et al., 2012). Therefore, the CF-NPs is expected to improved biological activity. By evaluating the porosity measurements, it can be found that the surface area of the CF-NPs is greater than the MCF-NPs. This can be accredited to the increase in crystallite size by introduction Mg ion (Jaimy et al., 2012). Both are classified as a mesoporous as pore diameter were less than 50 nm and would be valuable for better biological activities (Naikoo et al., 2016).

Besides the basic information about the fabricated ferrites nanostructures, the core objective of the current study was to explore the cytotoxic properties against human breast (MCF-7) cancer cells by MTT assay and their ROS properties. It was found that the viability cells are dose dependent (Mosmann 1983;

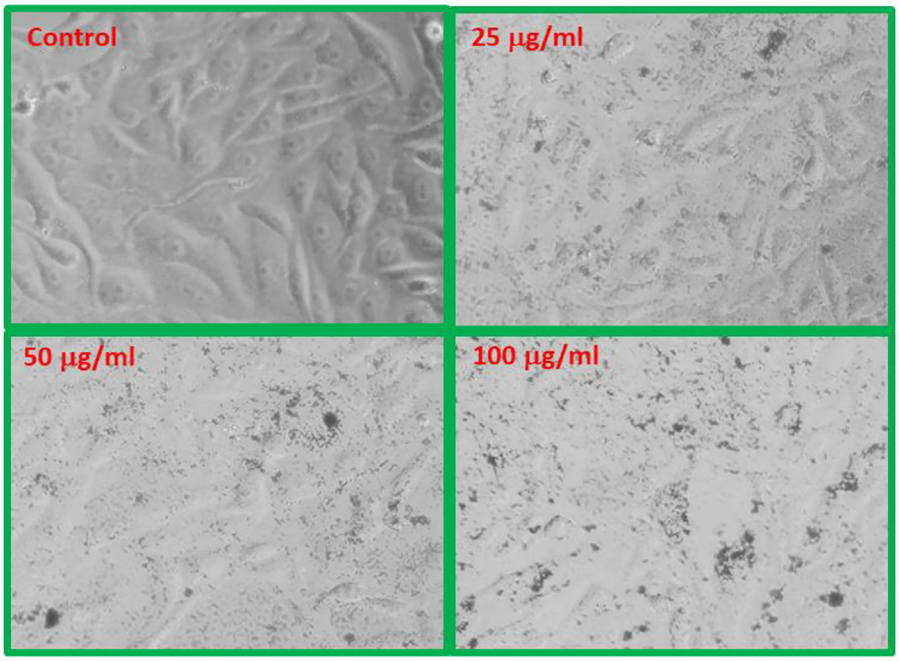

Fig. 9. MCF-NPs induced morphological changes in MCF-7 cells.

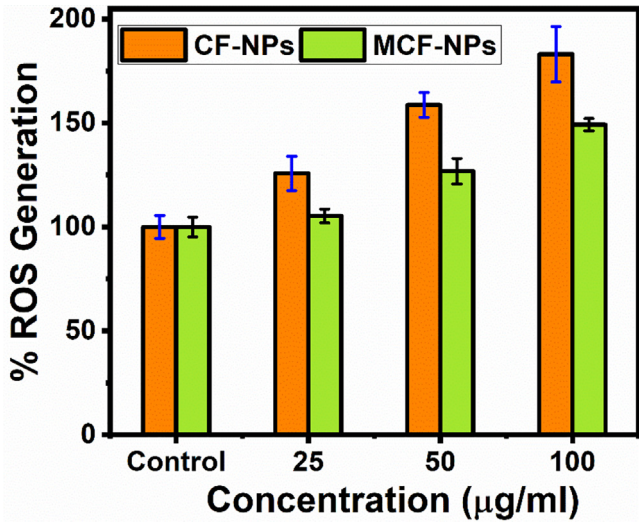

Fig. 10. ROS generation by ferrites NPs against in MCF-7. The experiments were conducted in triplicate manner (Mean ± SD triplicate).

Hathout et al., 2017). Although there are few literatures available on ferrites NPs cytotoxicity till date, the present cytotoxicity results are in similar agreement with the previous findings therein decreased of cell viability within these concentrations range by the exposure to different kinds of NPs (Hathout et al., 2017). Based on these observations, several hypotheses related to the entrance of NPs towards cancer cells, geometry, size, and distinctive property of NPs were responsible for the cell death (Mosmann 1983; Hathout et al., 2017; Coccini et al., 2010). As per the previous study, cell membranes exhibit small pore like passages which facilitates to enter NPs in to cells and damaged the upper layer of cell membrane (Coccini et al., 2010). In other reports, the nano structures can be easily entered in to the cells cytoplasm and react with cell's organelles and diminished the growth of cancer cells. Further, morphological changes in cancer cell in presence of NPs are good agreement with previous findings (Siddiqui et al., 2013; Stolle et al., 2005).

Additionally, to know cytotoxicity of cancer cells and the role of ferrites in mechanism, also measured the reactive oxygen species (ROS) for 24 h. It was considered that the production ROS by interaction of ferrites play the key role in mechanism of cytotoxicity because they can directly disturb the many components of cells such as DNA structure, proteins and lipids which in turn prime cause of cell death (Oberdorster et al., 2005). Consequently, our dose dependent finding and upsurge rate of ROS generation are well supported by the literature (Peter et al., 2014).

5. Conclusion

This investigation demonstrated that ferrite nanoparticles were successfully synthesized by green method using turmeric and characterized well with sophisticated instruments. The obtained results showed that formation of the crystalline ferrites with spherical shape. Moreover, the MTT cytotoxicity assay was performed from low (10 µg/ml) to high concentration (100 µg/ml) and result showed concentration dependent activity against MCF-7 human breast cancer cell lines which are agreed with the microscopic data. The obtained results shown that the CF-NPs induces more cytotoxicity as compare to MCF-NPs. Also these NPs are capable to induce ROS generation in MCF-7 cells and are accountable for cell death. The changes in the morphology of MCF-7 cells induced by NPs clearly exhibited cell death. From the obtained results it's concluded that the ferrites NPs are clearly enter into the cells and inhibit proliferation of cancer cells. Consequently, the synthesized cobalt ferrite NPs can be better explored in the near future for various biomedical, industrial and agricultural applications. From the obtained results and their observations, it's believed that the nanotechnology especially, the nanodoped materials are the better option due to their small diameter, high surface properties with enhance band gap, facilitates the better interaction of cells and their organelles and provide good results against cancer. These nanomaterials can be possible to reduce to cost of the treatment of cancer and will be helpful for

the deprived or low income families, who cannot afford the treatment cost.

Declaration of Competing Interest

The authors declare that they have no known competing financial interests or personal relationships that could have appeared to influence the work reported in this paper.

Acknowledgment

Appreciation to the Deputyship for the Research & Innovation, Ministry of Education in Saudi Arabia for funding this research work through the project no (IFKSURG-2-435).

Appendix A. Supplementary material

Supplementary data to this article can be found online at https://doi.org/10.1016/j.jksus.2023.102708.

References

Amiri, S., Shokrollahi, H., 2013. Magnetic and structural properties of RE doped Co-ferrite (REâ Nd, Eu, and Gd) nano-particles synthesized by co-precipitation. J. Magn. Magn. Mater. 345, 18–23.

Andrade, R.G.D., Veloso, S.R.S., Castanheira, E.M.S., 2020. Shape Anisotropic Iron Oxide-Based Magnetic Nanoparticles: Synthesis and Biomedical Applications. Int. J. Mol. Sci. 1, 2455.

Ashour, A.H., El-Batal, A.I., Maksoud, M.I.A.A., El-Sayyad, G.S., Labib, S., Abdeltwab, E., El-Okr, M.M., 2018. Antimicrobial activity of metal-substituted cobalt ferrite nanoparticles synthesized by sol–gel technique. Particuology. 40, 141–151.

Bray, F., Jemal, A., Grey, N., Ferlay, J., Forman, D., 2012. Global cancer transitions according to the Human Development Index (2008–2030): a population-based study. Lancet Oncol. 13, 790–801.

Carta, D., Casula, M.F., Falqui, A., Loche, D., Mountjoy, G., Sangregorio, C., Corrias, A., 2009. A Structural and Magnetic Investigation of the Inversion Degree in Ferrite Nanocrystals MFe_2O_4 (M = Mn Co, Ni). J. Phys. Chem. C 113, 8606–8615.

Casbeer, E., Sharma, V.K., Li, X.Z., 2012. Synthesis and photocatalytic activity of ferrites under visible light: A review. Sep. Purif. Technol. 87, 1–4.

Chen, K., Wei, J., Ge, C., Xia, W., Shi, Y., Wang, H., Jiang, X., 2020. Application of autoplanning in radiotherapy for breast cancer after breast conserving surger. Sci. Rep. 10, 10927.

Coccini, T., Roda, E., Sarigiannis, D.A., Mustarelli, P., Quartarone, E., Profumo, A., Manzo, L., 2010. Effects of water-soluble functionalized multi-walled carbon nanotubes examined by different cytotoxicity methods in human astrocyte D384 and lung A549 cells. Toxicology 269, 41–53.

Das, N.S., Ghosh, P.K., Mitra, M.K., Chattopadhyay, K.K., 2010. Effect of film thickness on the energy band gap of nanocrystalline CdS thin films analyzed by spectroscopic ellipsometry. Phys. E. 42, 2097–2102.

Hathout, A.S., Aljawish, A., Sabry, B.A., El-Nekeety, A.A., Roby, M.H., Deraz, N.M., Soher, E., Aly, S.E., Wahhab, M.S.A., 2017. Synthesis and characterization of cobalt ferrites nanoparticles with cytotoxic and antimicrobial properties. J. Appl. Pharm. Sci. 7, 86–92.

Issa, B., Obaidat, I.M., Albiss, B.A., Haik, Y., 2013. Magnetic nanoparticles: surface effects and properties related to biomedicine applications. Int. J. Mol. Sci. 14, 21266–21305.

Jaimy, K.B., Baiju, K.V., Ghosh, S., Warrier, K.G.K., 2012. Photocatalytic activity enhancement in doped titanium dioxide by crystal defects. Dalton Trans. 41 (16), 4824–4832.

Jha, A.K., Prasad, K., 2012. Biological synthesis of cobalt ferrite nanoparticles. Nanotechnol. Dev. 2 (1).

Jia, Z., Ren, D., Zhu, R., 2012. Synthesis, characterization and magnetic properties of $CoFe_2O_4$ nanorods. Mater. Lett. 66, 128–131.

Kombaiah, K., Vijaya, J.J., Kennedy, L.J., Bououdina, M., Ramalingam, R.J., Al-Lohedan, H.A., 2018. Okra extract-assisted green synthesis of $CoFe_2O_4$ nanoparticles and their optical, magnetic, and antimicrobial properties. Mater. Chem. Phys. 204, 410–419.

Kumar, L., Kumar, P., Narayan, A., Kar, M., 2013. Rietveld analysis of XRD patterns of different sizes of nanocrystalline cobalt ferrite. Int. Nano Lett. 8, 1–12.

Mathew, D.S., Juang, R.S., 2007. An overview of the structure and magnetism of spinel ferrite nano particles and their synthesis in microemulsions. Chem. Eng. J. 129, 51–65.

Monogr., Natl. Bur. Stand. (U.S.) 1971. 25, 9, 22.

Moradiya, M.A., Khiriya, P.K., Khare, P.S., 2021. Green synthesis of $CoFe_2O_4$ ferrofluid: Investigation of structural, magnetic and rheological behavior. Asian J. Nano Sci. Mater. 4, 263–273.

Mosmann, T., 1983. Rapid colorimetric assay for cellular growth and survival: application to proliferation and cytotoxicity assays. J. Immunol. Methods 65, 55–63.

Naikoo, G.A., Thomas, M., Ganaie, M.A., Sheikh, M.U.D., Bano, M., Hassan, I.U., Khan, F., 2016. Hierarchically macroporous silver monoliths using Pluronic F127: facile synthesis, characterization and its application as an efficient biomaterial for pathogens. J. Saudi Chem. Soc. 20, 237–244.

Nardin, S., Mora, E., Varughese, F.M., Avanzo, F.D., Vachanaram, A.R., Rossi, V., Saggia, C., Rubinelli, S., Gennari, A., 2020. Breast cancer survivorship, quality of life, and late toxicities. Front. Oncol. 10, 864.

Oberdorster, G., Maynard, A., Donaldson, K., Vincent, C., Julie, F., Kevin, A., Janet, C., Barbara, K., Wolfgang, K., David, L., Stephen, O., Nancy, M.R., David, W., Yang, H., 2005. Principles for characterizing the potential human health effects from exposure to nanomaterials: elements of a screening strategy. Part. Fibre Toxicol. 2, 8.

Peter, P. F., Qingsu., Huey-Min, Hwang., Paresh, C. Ray., Hongtao. Yu., 2014, Mechanisms of nano toxicity: generation of reactive oxygen species. J. Food Drug Anal. 22(1), 64–75.

Pon-On, W., Charoenphandhu, N., Tang, I.M., Jongwattanapisan, P., Krishnamra, N., Hoonsawat, R., 2011. Encapsulation of magnetic $CoFe_2O_4$ in SiO_2 nanocomposites using hydroxy apatite as templates: a drug delivery system. Mater. Chem. Phys. 131, 485–494.

Prasanna, G.D., Ashok, R.L., Prasad, V.B., Jayanna, H.S., 2015. Synthesis and characterization of magnetic and conductive nickel ferrite-polyaniline nanocomposites. J. Compos. Mater. 49, 2649.

Siddiqui, M.A., Alhadlaq, H.A., Ahmad, J., Al-Khedhairy, A.A., Musarrat, J., Ahamed, M., 2013. Copper oxide nanoparticles induced mitochondria mediated apoptosis in human hepatocarcinoma cells. PLoS One 8, 69534.

Stolle, L.B., Hussain, S., Schlager, J.J., Hofmann, M.C., 2005. In vitro cytotoxicity of nanoparticles in mammalian germline stem cells. Toxicol. Sci. 88, 412.

Taj, M. B., Alkahtani, M. D. F., Raheel, A., Shabbir, S., Fatima, R., Aroob, S., Yahya, R., Alelwani, W., Alahmadi, N., Abualnaja, M., Noor, S., Ahmad R. H., Alshater, H., 2021, Bioconjugate synthesis, phytochemical analysis, and optical activity of $NiFe_2O_4$ Nanoparticles for the removal of ciprofloxacin and Congo red from water, Sci. Rep. 11, 5439.

Tehrani, F.S., Daadmehr, V., Rezakhani, A.T., Akbarnejad, R.H., Gholipour, S., 2012. Structural, magnetic, and optical properties of zinc- and copper-substituted nickel ferrite nanocrystals. J. Supercond. 25, 2443.

Villete, C., Tailhades, P., Rousset, A., Kulkarni, G.U., Kanan, K.R., Rao, C.N.R., Lenglet, M., 1998. Cation migration and coercivity in mixed copper–cobalt spinel ferrite powders. J. Solid State Chem. 141, 56.

Wahab, R., Siddiqui, M.A., Saquib, Q., Dwivedi, S., Ahmad, J., Musarrat, J., Al-Khedhairy, A.A., Shin, H.S., 2014. ZnO nanoparticles induced oxidative stress and apoptosis in HepG2 and MCF-7 cancer cells and their antibacterial activity. Colloids Surf. B Biointerfaces 117, 267–276.

West, A.R., 1984. Solid State Chemistry and Its Applications. John Wiley & Sons, London.

Wu, M., Huang, S., 2017. Magnetic nanoparticles in cancer diagnosis, drug delivery and treatment. Mol. Clin. Oncol. 7, 738–746.

You, C., Han, C., Wang, X., Zheng, Y., Li, Q., Hu, X., Sun, H., 2012. The progress of silver nanoparticles in the antibacterial mechanism, clinical application and cytotoxicity. Mol. Biol. Rep. 39, 9193–9201.

Zutic, I., Fabian, J., Sarma, S.D., 2004. Spintronics: Fundamentals and applications. Rev. Mod. Phys. 76, 323–410.